ORIGINAL PAPER

CrossMark

Computational Modelling of Groundwater Inflow During a Longwall Coal Mining Advance: A Case Study from the Shanxi Province, China

Yuedu Chen[1,2] · A. P. S. Selvadurai[2] · Weiguo Liang[1]

Abstract

The paper investigates groundwater inflow into a longwall working face of the Xiegou Coal Mine located in the northwest of the Shanxi province, China. Three modelling approaches, including basic Darcy modelling, full poroelastic modelling using Biot's classical theory, and the full Biot poroelastic modelling that takes into account permeability alterations of the coal seam and strata due to alterations in the mining-induced stress state, are used to estimate the fluid flow into the underground longwall coal mine as the excavation progresses. Based on plausible assumptions of hydrogeological structure, boundary conditions and mining conditions, a three-dimensional finite element model of the simplified geological setting is developed using the COMSOL software. The permeability changes in both the strata and the coal seam due to the mining are associated with the mining-induced stress changes and water pressure, and the correlation between them accords with the exponential relationship. The differences in the modelling results of three approaches were analyzed, and the simulation results are compared with the field measurements.

Keywords Groundwater flow · Biot poroelasticity · Permeability alterations due to stress changes · Computational modelling

List of Symbols

K_D Bulk modulus the skeleton
G_D Shear modulus of the skeleton
p Pore fluid pressure
$\boldsymbol{\varepsilon}$ Infinitesimal strain tensor
$\mathbf{I}$ Identity tensor
α Biot coefficient
K_S Bulk modulus of the material composing the porous skeleton
$\mathbf{F}$ Body force vector
$\mathbf{u}$ Displacement of the solid skeleton
$\mathbf{v}^f$ Fluid velocity vector
$\mathbf{v}^s$ Solid velocity vector
K Permeability
η Dynamic viscosity of water
ν_u Undrained Poisson's ratio
ν Skeletal Poisson's ratio
$\tilde{B}$ Pore pressure parameter
β Stress sensitivity coefficient

✉ Yuedu Chen
  reading0901@163.com

1   College of Mining Engineering, Taiyuan University of Technology, Taiyuan 030024, Shanxi, China

2   Department of Civil Engineering and Applied Mechanics, McGill University, 817 Sherbrooke Street West, Montréal, QC H3A 0C3, Canada

1 Introduction

Coal represents a significant component of the energy production and mining in several countries, including China, USA, India, Russia, Australia and several other European nations. The large-scale coal exploitation and utilization provided great economic benefit while causing serious environmental consequences including mining subsidence, land desertification, water and soil loss and climate change due to greenhouse gases (GHGs). As shown in Fig. 1, in China, the extraction of coal always takes place in regions where groundwater is in abundance (Sun et al. 2012), hence the severe surface and underground water resource loss issues due to mining have become a topic of concern to coal mining industries. More importantly, the increasing use of the longwall mining methods in coal mines, a rapid and high extraction ratio underground mining technique (Guo et al. 2009; Booth 2006), have aggravated the drainage of groundwater into excavations due to depressurization of aquifers

Fig. 1 Water and coal resource distribution in China in 2011 (Tan 2013)
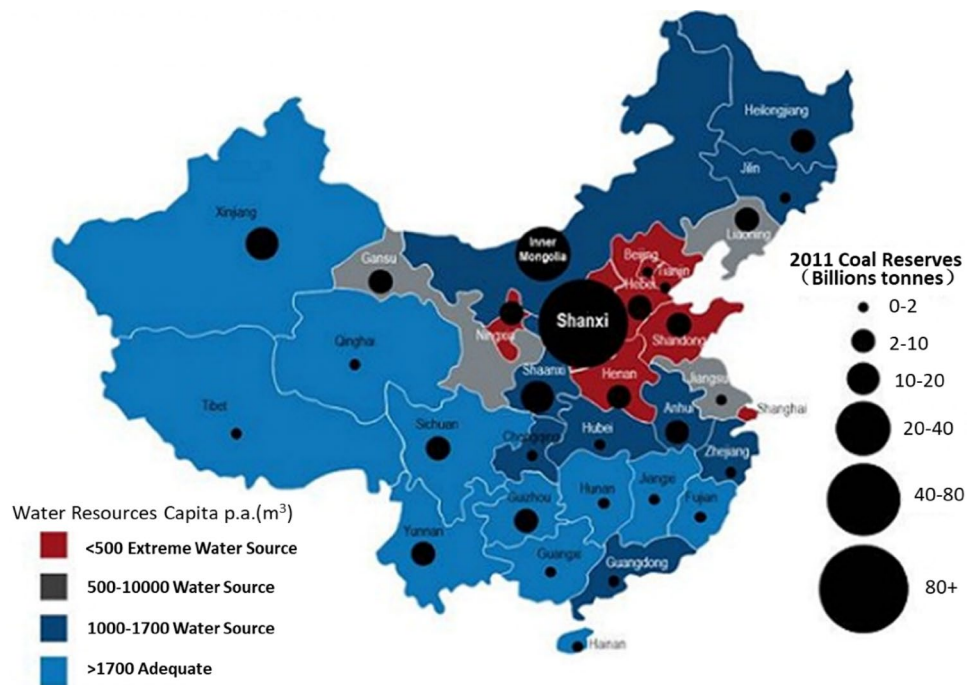
and also caused severe modification of hydraulic properties due to significant changes to the overburden stress (Kim et al. 1997). Thus, a clear understanding of the water inflow variation with the changes of hydrogeological and geomechanical behavior of the geological media around advancing longwall mining is essential to controlling and minimizing the mining-induced adverse impacts on water resource.

To investigate this issue, a number of field studies has been carried out over past few decades, including the observations of the mine water inflow variation with the longwall workings advancing (Wang and Park 2003; Zhu et al. 2014; Li et al. 2013; Zeng et al. 2017), the mining-induced water level fluctuation of aquifers (Zhang et al. 2010; Karaman et al. 2001; Booth et al. 1998), and the hydraulic conductivity response of overburden rock to longwall coal mining (Özgen Karacan and Goodman 2009; Aston and Singh 1983; Zhang et al. 2004). Although these field trials provide fundamental knowledge on changes in the hydrogeological behavior due to the longwall coal mining, the limited monitoring results cannot provide an adequate understanding of this problem. Thus, computational approaches, due to their convenience and flexibility to simulate complex hydrogeological conditions and non-linear material behavior, have been widely used to solve complex mining hydrogeological issues. A variety of numerical studies have been carried out in the modelling of mine water inflow into excavation disturbed regions under different mining stages based on the conventional groundwater flow model (Doulati Ardejani et al. 2003; Rapantova et al. 2007; Qiao et al. 2011; Surinaidu et al. 2014). These modelling approaches present

the conceptual understanding of the changes of groundwater flow pattern and natural drainage due to excavation morphology changes, and they are appropriate for the water balance calculation of the large scale of the underground mining (ranging up to thousands of square kilometers). However, such methods are not well suitable for application in the water inflow modelling into the longwall working because of the significant changes to the stress field caused by the mining, which can influence the water flow due to its coupling to the stress field. Thus, the full poroelastic model using Biot's classical theory, well known for its realistic characterization of the hydro-mechanical coupling behaviour of the deformable porous geologic rock mass (Biot 1941; Selvadurai 1996; Cheng 2015), has been widely used in describing the groundwater flow into the stress affected zone due to coal mine excavations (Kim et al. 1997; Liu and Hu 2007; Shi et al. 2017; Guo et al. 2009). In addition, the occurrence of damage zones of various intensity can lead to alterations in the permeability of the geologic strata, which can influence both the performance of the mine and the influx of water to the mining area. Thus, on the basis of the Biot's theory, the hydraulic conductivity alteration due to the mining-induced strata deformation and damage have received more attentions and been coupled into the full poroelastic model to evaluate the water flow into the advancing excavation regions (Ouyang and Elsworth 1993; Booth 1986; Kim et al. 1997; Zhu and Wei 2011; Zhu et al. 2014; Guo et al. 2012; Selvadurai and Shirazi 2004, 2005; Mahyari and Selvadurai 1998; Selvadurai 2004). All the above modelling approaches can be used to evaluate the water inflow

changes during longwall mining. However, the differences in the modelling results of these methods and the causes of these differences are not adequately investigated. In addition, the influence mechanism of mining-induced stress changes and hydraulic conductivity alteration of geologic strata on the water inflow are also not discussed, especially for three-dimensional situations. Thus, it is useful to develop a computational framework to compare several three-dimensional models of flow into a longwall excavation and to assess the impacts on groundwater inflow into a coal mine.

This paper presents three computational models of the mining operation to estimate the water inflow into the longwall excavated region. These various models include the basic Darcy modelling, a full poroelastic modelling using Biot's classical theory, and the full Biot poroelastic modelling that takes into account permeability alterations of the coal seam and strata due to alterations in the mining-induced stress state. To estimate the differences between these three methods in modelling the water inflow and to further understand the process of water flow into the advancing excavations, a specific case involving the No. 18112 working face of the Xiegou Coal Mine located in the northwest of the Shanxi province, where water influx presents a serious problem, was analyzed to compare these simulation results with field measurement results. In this study, a proper three-dimensional model of site practical situations was established based on the plausible assumptions of hydrogeological setting, boundary conditions, and mining conditions. Prior to the mining excavation, a steady-state model was established to investigate the groundwater flow system. The transient solver was taken into account to simulate the mining advancing rate in each excavation step. The permeability changes in both the strata and coal seam due to the mining are associated with alterations in mining-induced stress and water pressure, and the correlation between them accords with the exponential relationship. Besides, the sensitivity analysis of the flow influx variations to the stress sensitivity coefficient β, a critical parameter of the exponential relation, was conducted.

2 Modelling Framework

The groundwater inflow into the advancing longwall mine excavation is a complicated process mainly governed by the hydrogeological and geomechanical behaviors of several geologic media. Different modelling approaches, from the simple to the complex by considering poroelastic effects. Although various modelling methods usually come with different results, the comparison of these different numerical results will provide a gradual understanding of this complicated issue. The constitutive model and different modelling approaches for examining groundwater flow in a deforming and hydraulically evolving geological medium are given below.

2.1 Constitutive Model

The constitutive modelling of geomaterials and geomaterial interfaces is a well-developed area of research in geomechanics, focusing primarily on the study of the mechanical aspects (Christian and Desai 1977; Desai and Siriwardane 1984; Selvadurai and Boulon 1995; Davis and Selvadurai 2005; Pietruszczak 2010; Darve 2014; Cheng 2015). The focus on fluid transport aspects and coupled thermo-hydro-mechanical processes in fluid-saturated porous media has been initiated as a result of potential geologic sequestration activities related to the deep geologic disposal of heat-emitting waste materials. The research work in this area is extensive, and the account of recent developments is given in a recent volume by Selvadurai and Suvorov (2016). Coal-bearing rock formations are usually treated as sedimentary formations consisting mainly of the coal seam interbedded between sandstones with different grain sizes and other rocks such as mudstones (Bai and Elsworth 1991; Zhu and Wei 2011).

When considering poromechanical effects, the theory of Biot (1941) occupies a central position (Atkinson and Craster 1991; Yue and Selvadurai 1995; Selvadurai 1996, 2007; Cheng 2015; Selvadurai and Kim 2016; Selvadurai and Suvorov 2016). The development of the poroelastic part of the constitutive modelling adopts the procedures presented by Nguyen and Selvadurai (1995) and Selvadurai and Nguyen (1995) (see also Selvadurai and Suvorov (2012, 2014)) and the constitutive equation governing the poroelastic response is given by

$$\boldsymbol{\sigma} = 2G_{\mathrm{D}}\boldsymbol{\varepsilon} + \left(K_{\mathrm{D}} - \frac{2}{3}G_{\mathrm{D}}\right)\mathrm{tr}\,\boldsymbol{\varepsilon}\,\mathbf{I} - \alpha p\mathbf{I} \tag{1}$$

where K_{D} and G_{D} are, respectively, the bulk modulus and shear modulus of the skeleton; p is the fluid pressure; $\boldsymbol{\varepsilon}$ is the infinitesimal strain tensor; $\mathbf{I}$ is the identity tensor and α is the Biot coefficient defined by

$$\alpha = 1 - \frac{K_{\mathrm{D}}}{K_{\mathrm{S}}} \tag{2}$$

where K_{S} is the bulk modulus of the material composing the porous skeleton and Biot's concept for the effective stress follows from (1). The equation of equilibrium can be expressed in the form

$$G_{\mathrm{D}}\nabla^2\mathbf{u} + \left(K_{\mathrm{D}} + \frac{G_{\mathrm{D}}}{3}\right)\nabla(\nabla \cdot \mathbf{u}) + \alpha\nabla p + \mathbf{F} = \mathbf{0} \tag{3}$$

where $\mathbf{F}$ is a body force vector, and $\mathbf{u}$ is the displacement of the solid skeleton.

The fluid flow in the porous medium is described by Darcy's law, which takes the form

$$\mathbf{v}^f - \mathbf{v}^s = -\frac{K}{\eta}(\nabla p) \tag{4}$$

where $\mathbf{v}^f$ is the fluid velocity vector; $\mathbf{v}^s$ is the solid velocity vector; p is the pore fluid pressure; K is the permeability (units L^2) and η is the dynamic viscosity (units FTL^{-2}). The mass conservation equation for fluid-saturated poroelastic geomaterials can be written in various forms and here we adopt the expression

$$\frac{K}{\eta}\beta \nabla^2 p + \alpha\beta\frac{\partial}{\partial t}(\nabla \cdot \mathbf{u}) - \frac{\partial p}{\partial t} = 0 \tag{5}$$

where the parameters α and β can be expressed in the forms (Rice and Cleary 1976; Yue and Selvadurai 1995; Selvadurai 2004)

$$\alpha = \frac{3(\nu_u - \nu)}{\tilde{B}(1 - 2\nu)(1 + \nu_u)}; \beta = \frac{2G_D(1 - 2\nu)(1 + \nu_u)^2}{9(\nu_u - \nu)(1 - 2\nu_u)} \tag{6}$$

where ν_u is the undrained Poisson's ratio; ν is the skeletal Poisson's ratio and $\tilde{B}$ is the pore pressure parameter introduced by Skempton (1954) and defined by

$$\tilde{B} = \frac{\frac{1}{K} - \frac{1}{K_D}}{n\left(\frac{1}{K_f} - \frac{1}{K_D}\right) + \frac{1}{K} - \frac{1}{K_D}} \tag{7}$$

2.2 Stress-Induced Alterations in Permeability

A key aspect of the present paper is to examine the influence of modelling approaches on the groundwater influx into the coal mining excavation discussed in the previous section. The primary focus of the modelling is related to the stress-induced alterations in the permeability of the rocks encountered in the excavation region. In general, alterations to the geostatic stress field due to excavation processes can also alter the hydro-mechanical properties, but the dominant influence on fluid inflow into the excavation is expected to be responsible for any stress-induced alteration of permeability. The investigations of permeability alterations in various rocks, including granite, sandstone and limestone, are given by Shiping et al. (1994), Kiyama et al. (1996) and Selvadurai and Głowacki (2008, 2017) and further references to work in this area are given by Mahyari and Selvadurai (1998) and Selvadurai (2004). Glowacki and Selvadurai (2016) also discuss the influence of permeability alterations and use experimental data to develop a state space for permeability alterations with major and minor principal stresses. The fluid pressures that are applied to induce steady flow for permeability measurements are small enough that the externally applied principal stress state corresponds to the effective stresses. It should also be noted that the measure of permeability that can be obtained from the application of a tri-axial stress state is an effective value of the permeability of the altered rock that is subjected to axial flow. The experimental procedures have not advanced to the point that general anisotropy of the permeability alteration can be measured with accuracy. Currently, the general relationship between permeability evolution with stress has been expressed in the form (Zhao 2010)

$$K = K_0 \exp\left\{-\beta(I_1 - 3\alpha p)\right\} \tag{8}$$

where K_0 is the initial permeability; β is a stress sensitivity coefficient, and $I_1 = \text{tr}\sigma$.

2.3 Modelling Approaches of Flow into the Mining Excavation

The approach adopted in this study is to computationally examine the flow into a coal mining excavation as the excavation advances, and the modelling involves three procedures.

1. *Computational Modelling Approach I* is the reference case, which considers purely Darcy flow in the strata encountered, with the assumption that the permeability of the strata encountered is not influenced by the stress relief associated with the excavation process. Also, in this case, the effective permeabilities of the strata encountered are represented by equivalent values corresponding to the weighted harmonic mean K_v given by

$$K_v = \frac{\sum_{i=1}^{N} t_i}{\sum_{i=1}^{N} \frac{t_i}{K_i}} \tag{9}$$

where t_i and K_i correspond to the layer thicknesses and the layer permeabilities, and the *weighted mean* K_h, given by

$$K_h = \frac{\sum_{i=1}^{N} t_i K_i}{\sum_{i=1}^{N} t_i} \tag{10}$$

Combining with Eqs. (9) and (10), the effective permeability values corresponding to the strata above the coal seam and below the coal seam can be calculated. Other norms, including the *geometric mean* K_{GM}, can be developed by considering the research work of Selvadurai and Selvadurai (2010, 2014), where

$$K_{GM} = \sqrt[3]{K_v K_h^2} \tag{11}$$

2. *The Computational Modelling Approach II* In this case, the complete Biot poroelastic modelling of all the strata encountered in the vicinity of the mining excavation was adopted, i.e., (1)–(7), and the individual geomechanical properties of the strata are taken into consideration. In this approach, the permeability K is assumed to be uninfluenced by the alterations in the mining-induced stress state.

3. *The Computational Modelling Approach III* On the basis of approach *II*, changes to only the permeability K of the strata that result from changes to the stress state resulting from the mine excavation were taken into account. Prior to the excavation activities, the initial constant permeability K_0 in both the strata and coal seam were assigned to establish a steady-state model, and for each excavation step, K_0 was replaced with the variable permeability K, i.e., (8), which can be determined in the laboratory, to achieve the variations of the permeability as a result of alterations to the stress state (represented by the stress changes to the isotropic stress state) created by the mining operation. The above calculation procedures will converge to a stable condition through the iterations between the mechanical and fluid field employing simulation by numerical software.

3 Computational Modelling of the Case Study

To compare the differences of the above three modelling approaches in estimating the water inflow into the advancing longwall coal mine excavation, a specific case involving the No. 18112 longwall working face of the Xiegou Coal Mine located in the northwest of the Shanxi province was chosen.

3.1 The Geological and Hydro-geological Setting

The Xiegou coal mine is located in the northern part of the Hedong coal field, which is situated between the Yellow River and the Lüliang Mountains and is recognized as one of the six main coal fields in Shanxi Province, China (Fig. 2). The minefield stretches from the south to the north in a long strip configuration with a width of 4.5 km and length 22 km. Topographically, the study area is situated in the northeastern end of the Lüliang Mountains and possesses a varied topography that consists of numerous small rivers and denuded mountains. The undulating terrain contributes to high topographies in the north and south with low topographies in the central region. A large area of the survey region is covered by loose soil. The study area has a temperate continental monsoon climate, with an average annual precipitation of 625 mm. The Lanyi River, a tributary of the Yellow River, is the largest river flowing through the mining region from east to west.

The geotectonic feature of the study region is that it is situated at the eastern edge of the Ordos fault block and the regional geological setting is a slightly inclined monoclonal structure with an overall strike along the north–south axis with dips about 8° to the west (Fig. 3). The geological structures of the mining area are simple and stable with no obvious major fault structures or collapsed regions. Some minor faults were, however, discovered during mining operations. According to the geological evaluation of borehole data, the geological stratigraphy of the location of mining interest consists of Quaternary, Neogene, Triassic, Permian, Carboniferous and Ordovician sequences. The coal-bearing strata are located mainly within the Carboniferous-Permian sequences. The dominant mineable layers include the No. 8 coal seam of the Shangxi formation of the lower Permian (P_1sh) and the No. 13 coal seam of the Taiyuan formation of the upper Carboniferous (C_3t). In this study, attention is restricted to the No. 8 coal seam, with a dip angle of 7° and an average thickness of approximately 5.95 m, which is used in the modelling exercises.

The mining area is located in a loess hilly region with gullies formed by rainfall and erosion. The Lanyi River, the main watercourse that traverses the mining area, flows through the central region of the mining area from east to west and is approximately 9 km from the centreline of the starting excavation of the No. 18112 mine working face. Several other smaller rivers contribute seasonally to the groundwater conditions. The main aquifers in the mining area that influence the hydrogeology of the No. 8 coal seam, from bottom to top, are as follows: (1) the karst feature aquifer of the upper Majiagou formation in the Middle Ordovician, (2) the sandstone aquifer of the Taiyuan formation in the Carboniferous, (3) the sandstone aquifer of the Xiashihezi and Shanxi formations of the Permian, and (4) the alluvial porous aquifer in the Quaternary. Furthermore, the main aquicludes are located in the Taiyuan formation and the Benxi formation. According to the geological survey reports, these aquifers receive an influx of rainfall and surface water from the outcrops (Fig. 3). Also, the porous aquifers can also receive a lateral supply of water from aquifers with fissures. Since there is no evidence of dominant major faults or collapse columns in the mining area, the flow of groundwater is less influenced by such features and are controlled solely by the monoclinal structure. Also, the Ordovician confined aquifer is remote from the No. 8 coal seam and is not expected to contribute to water influx in the mining area of interest to the modelling. In general, the regional groundwater flow direction is similar to that of the surface groundwater flow pattern, which is from east to west.

Fig. 2 Location of the Xiegou coal mine and No. 18112 mining working faces [drawn using the Google earth version 7.1.8.3036]

3.2 Model Development

The mine working face associated with unit No. 18112 was adopted for the model development. Since the overall advancing length of the working face of the unit was approximately 3.8 km, it was not possible to model the entire excavation process; the excavation from the ground surface access to a progress length of 200 m was used in the model development. Furthermore, reliable field data is only available for this limited excavation advance length. The general layout of the mine region to be modelled is shown in Fig. 4. The three-dimensional geometry of the No. 18112 longwall working face of 600 m × 800 m × 197 m is shown in Fig. 4a

and was chosen as the representative domain for model development. In this model, a total of fifteen rock strata, divided into eight types by rock properties are modelled. These include the No.8 coal seam, the fine sandstone, the medium sandstone, the coarse sandstone, the mudstone, the confined aquifer, the unconfined aquifer and the loess, all indicated in different colours; however, the sandstones with different grain sizes shown in Fig. 4a, are uniformly represented in a brown colour in the model schematic (Fig. 4b).

Assuming a symmetric configuration of the mining panel in the advancing direction, only half the domain is modelled (Fig. 4b) to establish the computational domain. Figure 4c shows the mesh refinement of one-half of the No. 18112
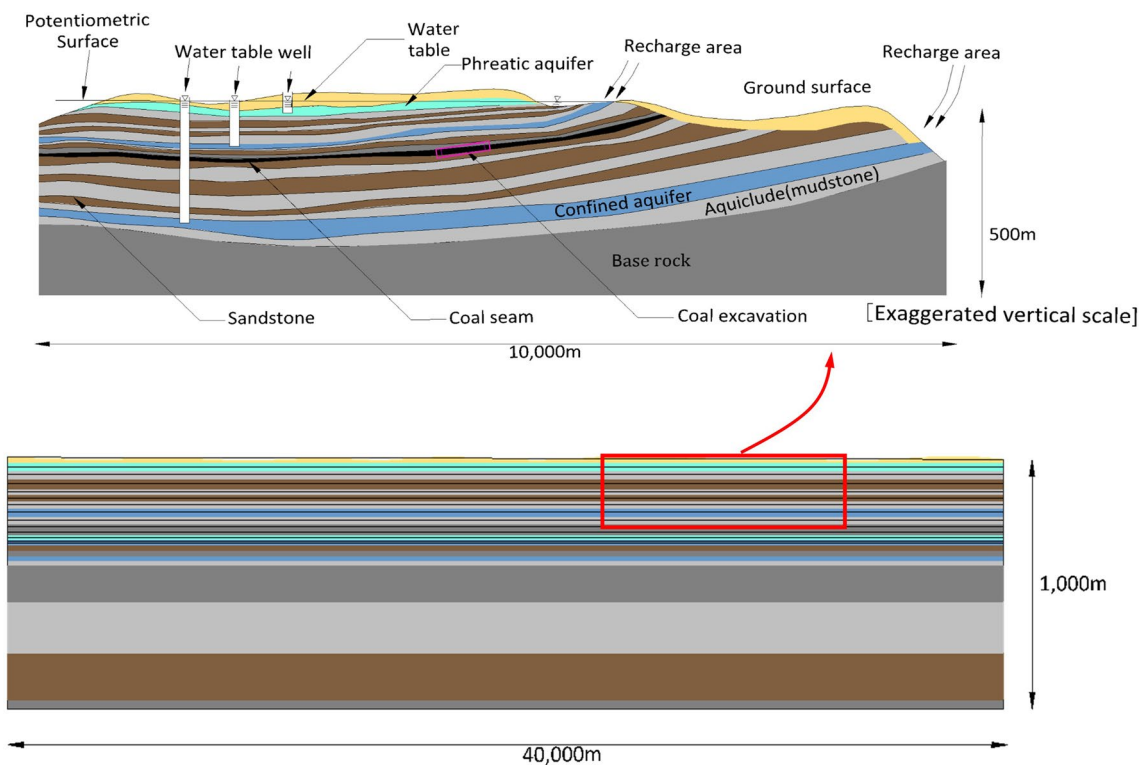
Fig. 3 The geological profile schematic of the mining area

working face used to develop the computational model using COMSOL™ Multiphysics Code, with dimensions of 600 m × 400 m × 197 m in the x, y and z-directions, respectively. A total of 61,600 hexahedral elements were used, and mesh refinement is employed at regions close to the excavation to better estimate the fluid influx and alterations in the stress state.

3.3 Boundary and Initial Conditions

Based on the long-term monitoring of groundwater levels in boreholes located in the vicinity of the western boundary of the working face, the piezometric level in the overlying fissured sandstone aquifer is approximately 1050 m, which corresponds closely to the ground elevation. Therefore, prior to the mining activities, the initial hydrostatic head in the region is taken to correspond to the ground level, and the datum plane required for the modelling is taken as the plane $Z = 0$ shown in Fig. 5. The boundary $X = 0$ corresponds to a plane of symmetry in the modelling exercise. In this regard, (1) null Neumann boundary conditions are prescribed with respect to the hydraulic potential, (2) null conditions are prescribed on the normal displacements and (3) null conditions are prescribed on the shear tractions. Similarly, the base plane $Z = 0$ is assumed to be impervious, frictionless and non-deformable; accordingly, the boundary conditions

for the hydraulic potential, the displacements, and the shear tractions are the same as those for the plane of symmetry. The free surface of the modelled domain has a constant total head of 197 m corresponding to the borehole water level records and considered to be free of tractions. As excavation progresses, the boundary surface of the excavated region is prescribed with a zero pressure head and zero tractions. The modelling does not take into consideration the geometry changes associated with the mining excavations. In addition, mechanical hydraulic supports used for longwall roof supporting are also ignored since the footprint of these constructions is small in relation to the surface area of the excavated region. A schematic view of the domain is shown in Fig. 5. The site has no tectonic anomalies; the in situ stress state prior to the mining operations is prescribed to be geostatic with the lateral stresses in the region governed by the elastic Poisson's ratio of the skeletal material.

3.4 Simulation of Excavation Sequences

The mine excavation is assumed to progress in 13 steps, with approximately 10 m/step from 0 to 60 m and 20 m/step from 60 to 200 m. The excavation progressed at approximately 3.33 m/day. The simulated excavation sequences require step-wise changes in the hydraulic and traction boundary conditions on the excavation surface. Ideally, the excavation
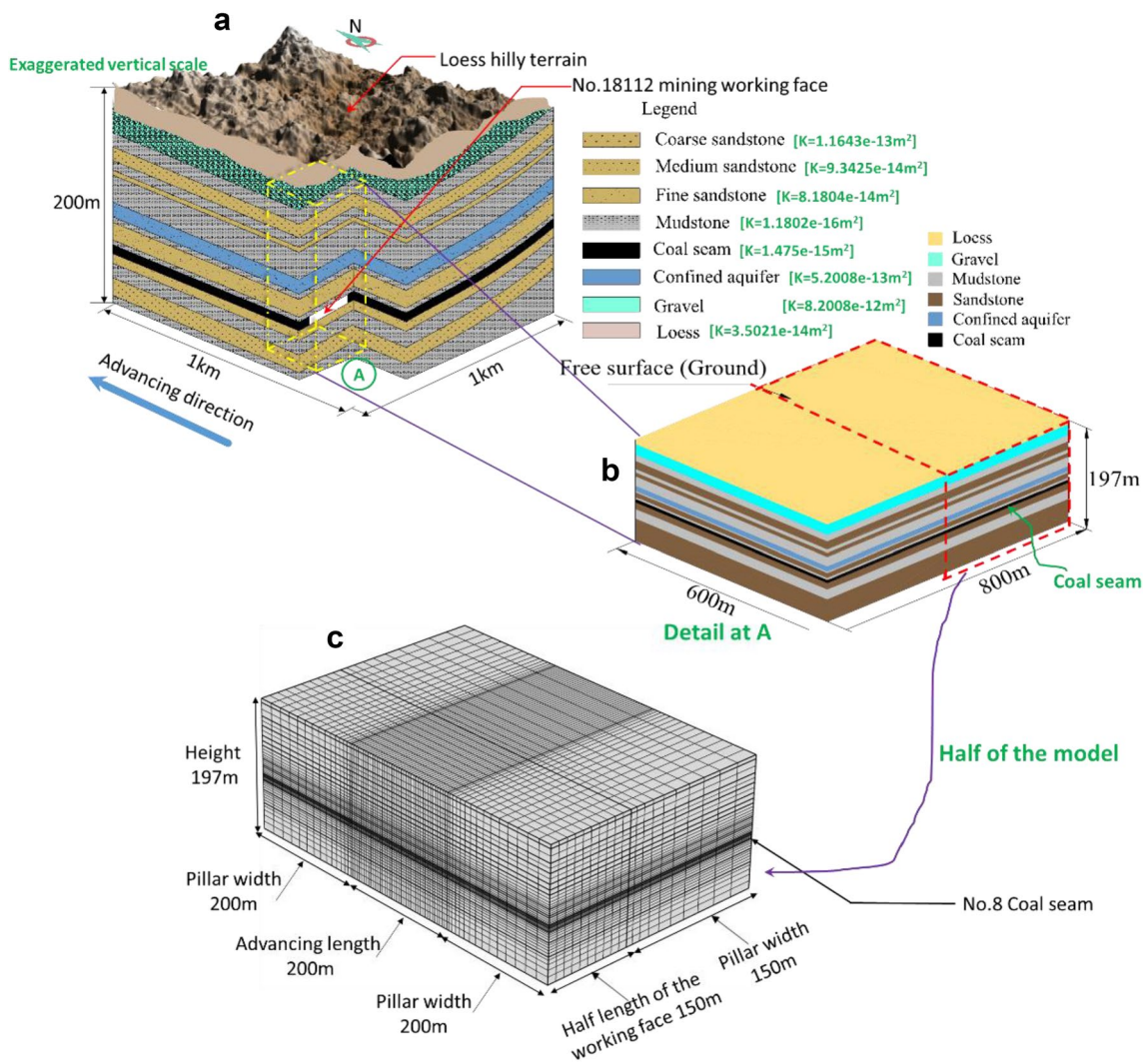
Fig. 4 A three-dimensional schematic view of the geological setting and the meshing configuration used to model the No. 18112 mining working face
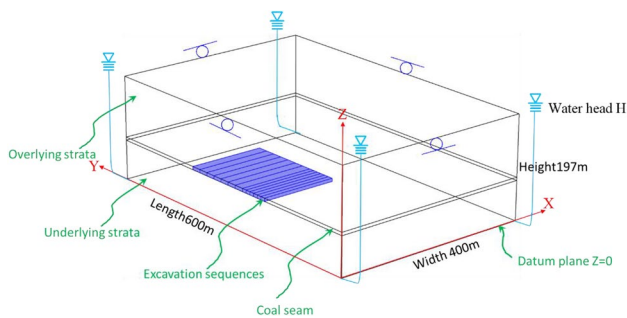

Fig. 5 Hydraulic, displacement and traction boundary conditions used in the computational modelling

process is a moving boundary problem that requires continual changes to the boundary conditions and the documentation of the residual hydraulic head and stress state prior to the commencement of the subsequent excavation stage. In this modelling exercise, the hydraulic head and the stress state in the domain are assumed to reach a steady state at the end of each excavation sequence. This reduces the computational rigor of the modelling and is a useful approximation of the influences of the excavation process. The simulated excavation sequences are shown in Fig. 6.

3.5 The Geomechanical and Hydrogeological Parameters

The mine excavation site targeted for modelling and the range of modelling exercises requires several hydraulic and mechanical parameters applicable to all the strata encountered, including the variation of the parameters as a result of alterations to the stress state created by the mining operation. It is not easy to estimate the material parameters required
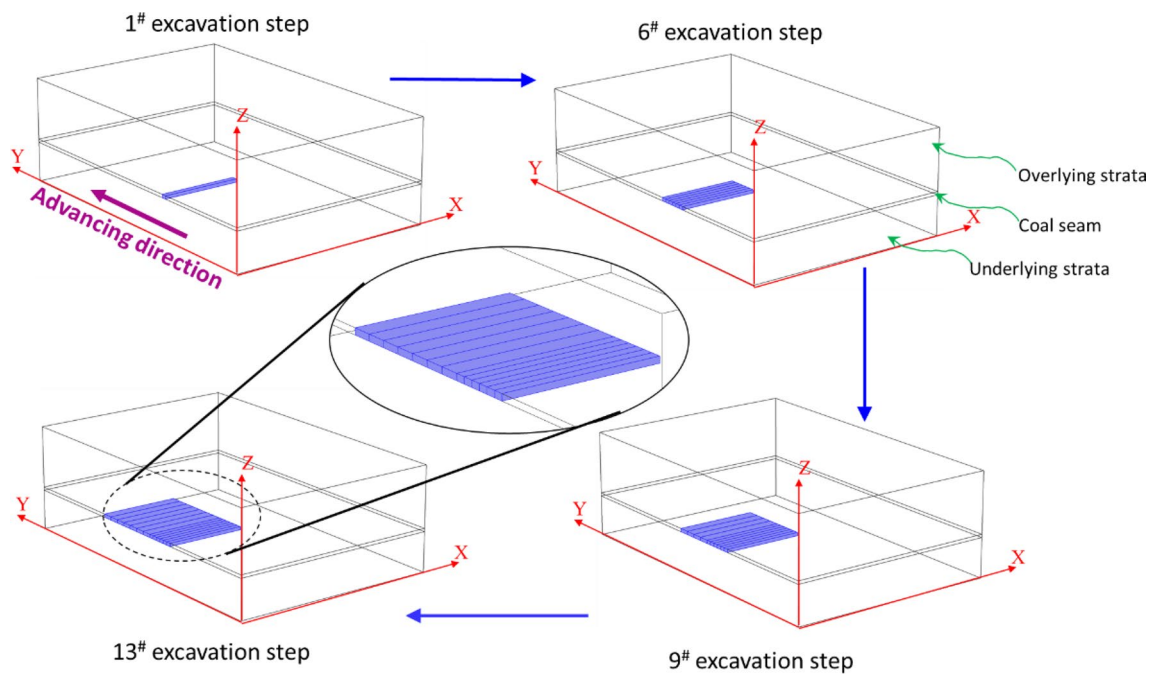
Fig. 6 The mine excavation sequences used in the modelling

for a mining operation on the scale of a geological setting indicated in Figs. 3 and 4. While some parameters, particularly for the sandstone components, can be determined in the laboratory, the material parameters for other rocks, including the coal, were determined by consulting published literature. This is a limitation of the study but this deficiency can be improved with more site-specific geomaterial testing. The basic in situ (i.e., pre-mine excavation) elastic modulus (E), Poisson's ratio (ν) and uniaxial compression strength (UCS) applicable to sandstones with different grain sizes were determined in the laboratory (Fig. 7a; Table 1) and corresponding data for rocks such as mudstone, gravel, and loess were obtained from published literature (Guo et al. 2012). Of necessity, the mechanical and hydraulic parameters of the rock encountered at the mine site are assumed to be homogeneous and isotropic. The penalty for incorporating non-homogeneity and anisotropy can effectively make the computational modelling exercise unmanageable. The permeability parameters applicable to the rocks encountered at the mine site were also estimated in a similar way. It is also possible to adopt effective permeability measures based on the "Geometric Mean Concept", if there is evidence of moderate departures from hydraulic isotropy (Selvadurai and Selvadurai 2010, 2014).

The other poroelasticity parameters, including the mass density ρ, porosity n and Biot coefficient α, that are necessary for poroelastic modelling were obtained from related references (Zhao 2010). More advanced approaches for estimating the Biot coefficient by taking into consideration the

mineralogical composition of the rock fabric have recently been proposed by Selvadurai (2018), although such techniques require extensive laboratory investigations at several scales of interest. The set of material and physical parameters that were used in the computational modelling is presented in Table 2.

For the computational modelling approach *I*, the effective permeabilities K_v and K_h should be determined. Combing with Eqs. (9) and (10), the effective permeability values corresponding to the strata above the coal seam and below the coal seam are summarized in Table 3.

For the computational modelling approach *III*, the stress sensitivity coefficient β should be identified for different geological media. In this case, we focus on the variations of permeability applicable to different types of coal originating from the Shanxi province.

Figure 8a shows various empirical models describing stress-induced permeability alteration for different types of coal, where a certain coal was taken as an example to illustrate the experimental data. In this study, the stress-dependent permeability evolution obtained from tests conducted on a representative coal obtained from an adjacent mine gave the following result for Eq. (8): i.e.,

$$K = 1.4445 \, \exp\left\{-0.1224I_1 + 0.2017p\right\} \quad \text{m}^2 \tag{12}$$

and a Biot coefficient $\alpha \approx 0.55$. Here, the reason for adopting Eq. (12) from another mine is that this mine is very close to the Xiegou coal mine in this study, which can be seen Figs. 2, 8a. Besides, the type of the coal specimen used for
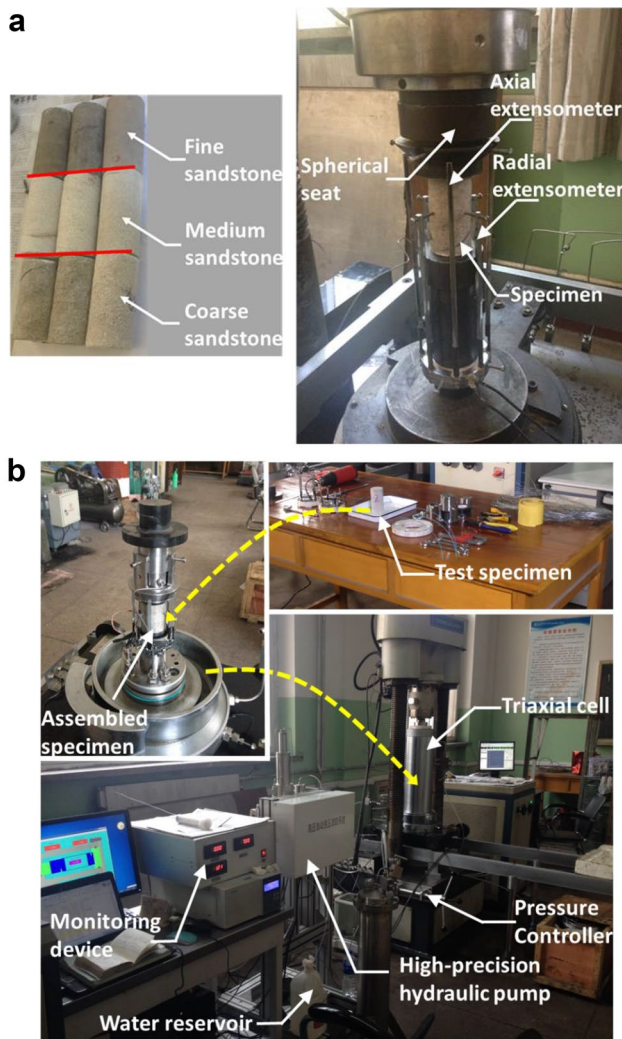
a

b

Fig. 7 Experimental configurations for estimating the mechanical and hydraulic parameters of the sandstones. **a** The uniaxial compression test, **b** the permeability measurement test under triaxial compressive stresses

testing to obtain Eq. (12) is the same as that of the No.8 coal seam in Xiegou coal mine, and both of them belong to the high-rank coal, bituminous coal and steam coal, respectively. Thus, the stress-dependent permeability relation describing using Eq. (12) is reasonable to use as representing that of the coal encountered in this study. Besides, laboratory investigations of stress-dependent permeability variations for the fine sandstone were conducted and the results are given in Fig. 8b. The expression for permeability variations with the first invariant of the effective stress tensor can be expressed in the form

$$K = 8.1804 \ \exp\left\{-0.04136 I'_1\right\} \ m^2 \qquad (13)$$

Also, the stress sensitivity coefficient for sandstone has been documented in numerous laboratory investigations (David et al. 1994; Zhang et al. 2016) and this information can be used to deduce the stress-sensitivity parameters, which are summarized in Table 2. The range for the stress-sensitivity coefficient β can vary from $(6.21 \ to \ 18.1) \times 10^{-3} \ MPa^{-1}$ to $(0.66 \ to \ 11.36) \times 10^{-3} \ MPa^{-1}$.

4 Modelling Results

The computational modelling was performed using the COMSOL™ Multiphysics Code. The use of this code for problems involving porous media flow and Biot poromechanics with stress-dependent alterations in the properties is well documented in the articles by Selvadurai and Suvorov (2012, 2014), Selvadurai et al. (2015) and Selvadurai and Najari (2016, 2017).
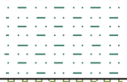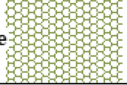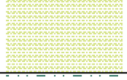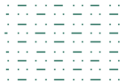
4.1 Results from the Modelling Approach I

Using only the Darcy flow model in the COMSOL™ Multiphysics Code, the rate of water flow into the excavation as the excavation distance increases was investigated first. Figure 9 shows the groundwater flow pattern of the cutting

Table 1 Uniaxial compression test results for sandstone specimens with different grain sizes

Rock type	Sample no.	Diameter D (mm)	Length L (mm)	UCS(MPa)	Poisson ratio λ	Elastic modulus E (GPa)
Fine sandstone	FS1	49.58	99.96	73	0.22	9.85
	FS2	49.56	99.84	72	0.27	9.56
	FS3	49.56	99.22	74	0.24	9.79
Medium sandstone	MS1	49.60	99.06	66	0.22	8.23
	MS2	49.60	98.02	69	0.21	8.56
	MS3	49.56	99.08	63	0.20	7.94
Coarse sandstone	CS1	49.60	95.62	63	0.32	8.21
	CS2	49.58	100.12	65	0.31	8.08
	CS3	49.60	98.96	57	0.33	7.65

Table 2 The material parameters used in the computational modelling

Lithology	Column Chart 1:200	No.	Thickness (m)	Poisson's ratio	Density (kg/m³)	Elastic modulus(GPa)	UCS (MPa)	Porosity	Biot's coefficient	Permeability (m²)	Stress sensitive coefficient β
Loose		1	6	0.27	1500	2.31	3	0.55	0.6	3.5021e-14	0.374
Gravel		1	20	0.35	1610	1.4	5	0.35	1	8.2008e-12	0.350
Mudstone		3	14	0.21	2080	4.1	28	0.25	0.6	1.1802e-16	0.072
Medium sandstone		4	15	0.29	2410	8.2	66	0.23	0.84	9.3425e-14	0.045
Mudstone		5	8	0.21	2080	4.1	28	0.25	0.6	1.1802e-16	0.072
Fine sandstone		6	7	0.25	2510	9.74	73	0.21	0.8	8.1802e-14	0.041
Mudstone		7	20	0.21	2080	4.1	28	0.25	0.6	1.1802e-16	0.072
Fine sandstone		8	9	0.27	2420	8.31	65	0.21	0.78	5.2008e-13	0.023
Mudstone		9	3	0.21	2080	4.1	28	0.25	0.6	1.1802e-16	0.072
Fine sandstone		10	11	0.25	2510	9.74	73	0.21	0.8	8.1802e-14	0.041
Mudstone		11	3	0.21	2080	4.1	28	0.25	0.6	1.1802e-16	0.072
No.8 coal seam		12	6	0.27	1400	2.31	17	0.25	0.55	1.457e-15	0.122
Fine sandstone		13	15	0.25	2510	9.74	73	0.21	0.8	8.1802e-14	0.041
Mudstone		14	20	0.21	2080	4.1	28	0.25	0.6	1.1802e-16	0.072
Coarse sandstone		15	40	0.31	2650	8.01	63	0.33	0.86	1.1643e-13	0.054

plane $X = 78$ m, located within the coal seam and chosen as the monitoring plane for the calculation of the flow rate. As expected, the maximum flow rate occurs in the vicinity of the corner regions of the excavation zone and remains at a value of 21.9×10^{-3} m³/h, which does not change as the mining excavation progresses. In Fig. 9, the color, from red to blue along a flow line, is used to represent the decrease of the pressure head, and the flow path of the groundwater. It can be seen that stress changes due to mining activities affect the flow direction of the underground water, and the corner regions always exhibit the largest flow rate.

4.2 Results from the Modelling Approach II

During mining of the longwall working face, a significant increase in the underground water flow rate will occur if the stress in the surrounding strata decreases. Thus, the complete poroelastic model is used to analyze the extent of stress relief, which will enable the linking of the estimation of the flow rate with changes in the stress state (Guo et al. 2012). To more clearly represent the magnitude of vertical stress

Table 3 The vertical and horizontal permeability

	Upper layer	Coal seam	Lower layer
Vertical permeability	2.85e16	1.41e−13	4.42e−16
Horizontal permeability	1.40e10	1.41e−13	4.52e−13
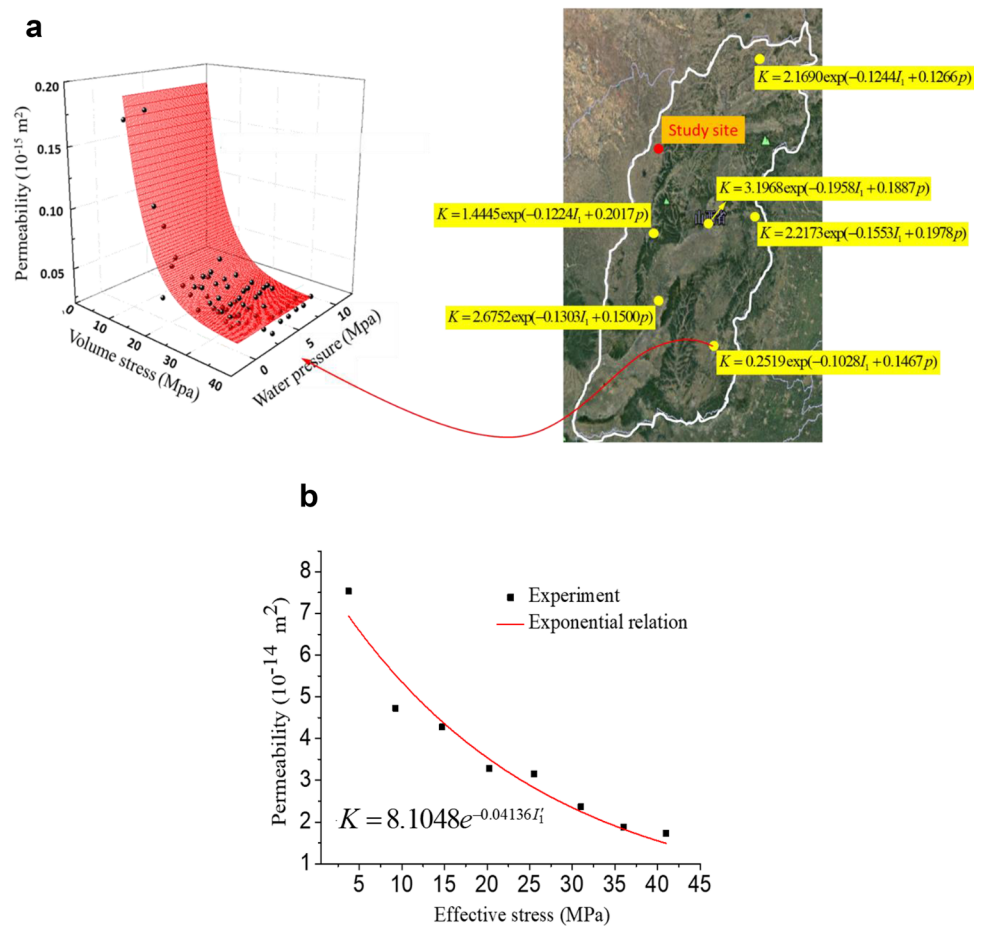
variation with the mining process at different locations in the surrounding rock, the variation rate of the vertical stress was used. It represents the ratio between the post-mining stress and the pre-mining stress, as defined below (Lu and Wang 2015). (In this modelling approach, the negative and positive values represent compression and tension, respectively.)

$$\sigma_R = \frac{\sigma_v - \sigma_v^0}{\sigma_v^0} \tag{14}$$

where σ_v and σ_v^0 denote the post- and pre-mining vertical stresses, respectively. Figure 10a shows the three-dimensional contours of the vertical stress variation rate σ_R within the roof and floor strata as the working face excavation progresses to 200 m. The stress distributions along the advancing direction and the length direction are plotted in Fig. 10b, c, respectively. It can be observed that the zone of relief of the vertical stress is mainly formed in the overlying and underlying strata located at the middle of the stope, and the regions that are far from the excavated space mainly have larger variations of σ_R.

It can be observed that the strata located in the front, back and on both sides of the excavated space show an increase in stress and have larger values within the strata closer to the stope. The main reason for the above changes is the transfer of the overburden weight in the excavated area to the surrounding rock (Lu and Wang 2015). The value of σ_R along the monitoring lines located on the floor ($X=0$, $Z=0$) and the roof strata ($X=0$, $Z=157$) with different advancing distances are shown in Fig. 11.

At each excavation step, the variation of σ_R can be divided into five-stages, increase–decrease–increase–decrease and stabilization. Correspondingly, the variation of the vertical stress shows a four-stage process, increase–decrease–increase–stabilisation, which confirms the results of Guo et al. (2012). According to Fig. 11, the curves move forward as the mining progresses, indicating that the adjustment stress of the surrounding strata at the head, back and sides of the working face increase gradually as the excavation distance increases. In contrast, the stress in the central part of the stope gradually recovers to the original stress as the mining progresses. These observations are of assistance in interpreting the anticipated stress-related changes in permeability in the geological setting as the mine excavation progresses.
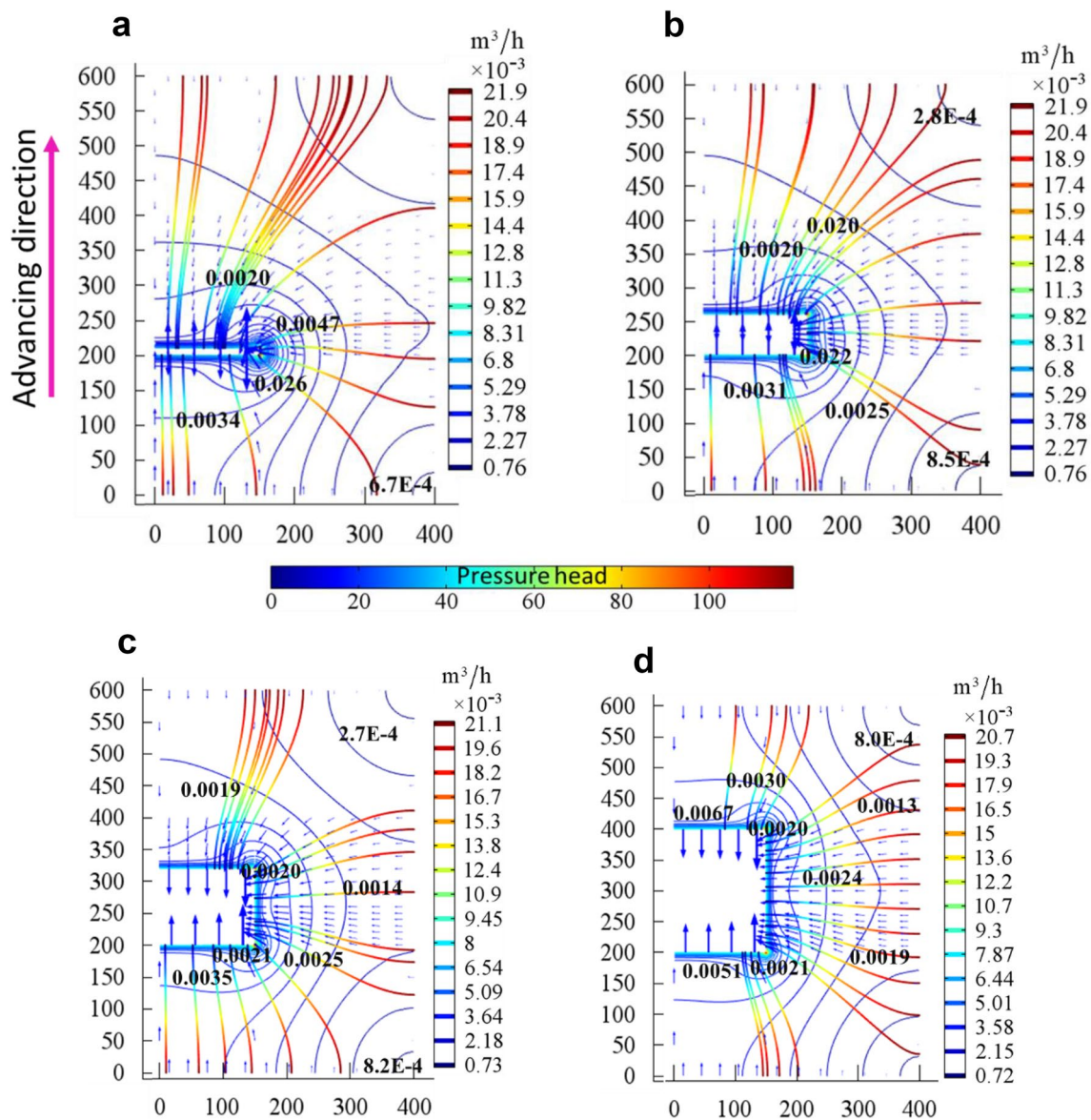
Fig. 9 Variations of the flow rate in section plane $X = 78$ located within the coal seam at different excavation distances, **a** 0 m, **b** 60 m, **c** 120 m, **d** 200 m. The colored flow lines also represent variations of the pressure head. (Color figure online)

4.3 Results from the Modelling Approach III

The permeability of the surrounding strata also influences the evolution of the flow rate as the mining advances. Thus, based on the approach *II*, changes to the permeability of the strata resulting from the alterations of the mining-induced stress state were taken into consideration. The variations of the permeability can be expressed in the logarithmic form (owing to the large difference of the permeability in various layers)

$$K_R = \frac{\log_{10}(K) - \log_{10}(K_0)}{\log_{10}(K_0)} \tag{15}$$

where K and K_0 are the post- and pre-mining permeabilities, respectively. The modelled three-dimensional distribution contour of K_R within the roof and floor strata as the working face advances to 200 m is plotted in Fig. 12a. The permeability distribution along the advancing direction and the working face length direction are also plotted in Fig. 12b, c, respectively. It can be seen that significant permeability increases develop in the de-stressed zone (caving zone), but its significance gradually diminishes and is restricted to a certain distance away from the excavation space, where the permeability begins to decrease. This pattern of permeability alteration was also computationally predicted by Głowacki and Selvadurai (2016) who examined the two-dimensional

Fig. 10 Modelled distribution contour of the vertical stress variation rate σ_R within the roof and floor strata when the working face excavation progresses to 200 m. **a** Three-dimensional distribution of the model, **b** two-dimensional distribution within the section plane $X=0$, **c** two-dimensional distribution within the section plane $Y=300$
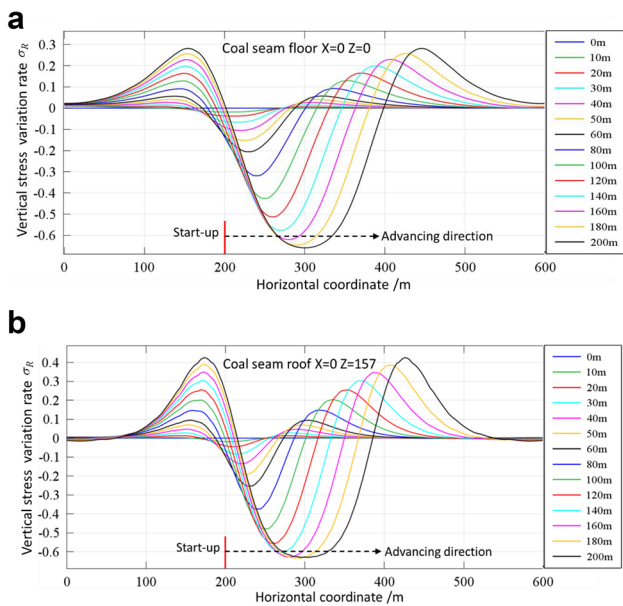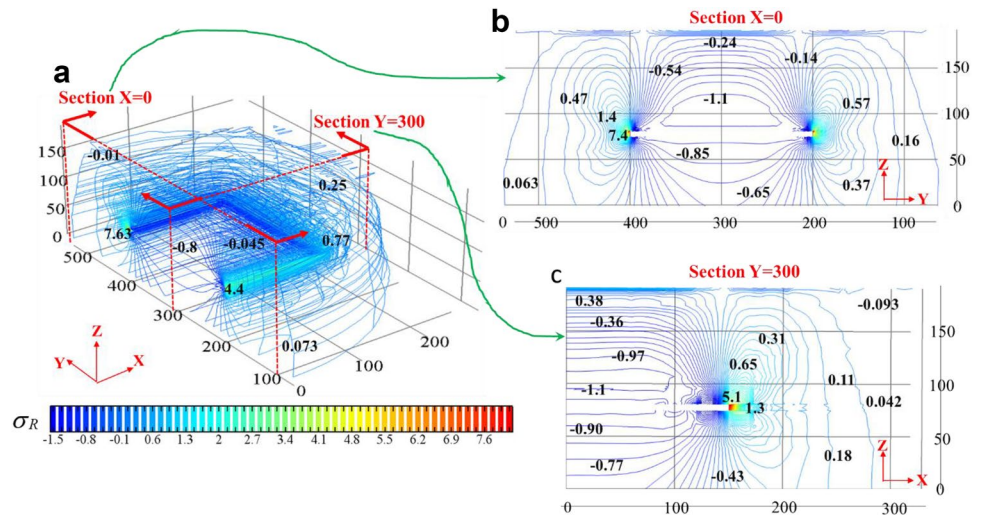

Fig. 11 Modelled vertical stress variation rate σ_R changes with the excavation distance from 0 to 200 m along the monitoring lines. **a** The monitoring line located within the floor strata ($X=0, Z=0$), **b** the monitoring line located within the roof strata ($X=0, Z=157$)

flow pattern into a circular tunnel. The simulated results of the permeability variation are compared to that of the mining-induced stress alterations, indicating that the permeability increase is closely related to the decrease of the mining-induced stress, resulting in greater permeability in the de-stressed zone. The permeability variation with increases in the excavation distances, which can be observed from the simulation results of the monitoring lines located on the floor strata ($X=0$, $Z=40$) and the roof strata ($X=0$, $Z=157$), are shown in Fig. 13. An increase in the distance mined will result in larger areas with significant permeability alterations within the overlying and underlying strata close to the

excavation, but it will have the opposite effect within the overlying strata that are remote from the excavation.

4.4 Comparisons Between Computational Results and In Situ Observations

In this section, the variations of computed fluid influx Q_c with duration of mining, calculated using the three computational approaches outlined previously, was compared with the measured field data Q_f, as shown in Fig. 14. The fluid influx Q_c was calculated as:

$$Q_c = \int_{t_0}^{t_1} \int_S \left[-\frac{K\gamma_w}{\mu} \nabla H \right] \mathbf{n} \, dA dt \tag{16}$$

where $\mathbf{n}$ refers to the outward unit normal vector associated with S. t_0 and t_1 represent the start and end time of each excavation sequence, respectively.

As seen in Fig. 14, although the computational values Q_f for various models all increase with duration of mining, their growth trends are different. The Q_c of model I (pure Darcy model) grows linearly and shows the largest difference from the field measurement Q_f compared to the other two models. Conversely, the Q_c of the model III (poroelasticity model with changes in K) showed the smallest difference from the Q_f, which first increases rapidly and then tends to grow steadily. To represent the difference between Q_f and Q_c more intuitively, the relative variation of flow influx Q_δ is introduced as:

$$Q_\delta = \frac{Q_c - Q_f}{Q_f}(\%) \tag{17}$$

where the larger the Q_δ, the greater the difference between Q_c and Q_f. The variations of Q_δ with increasing duration of mining are shown in Fig. 15.
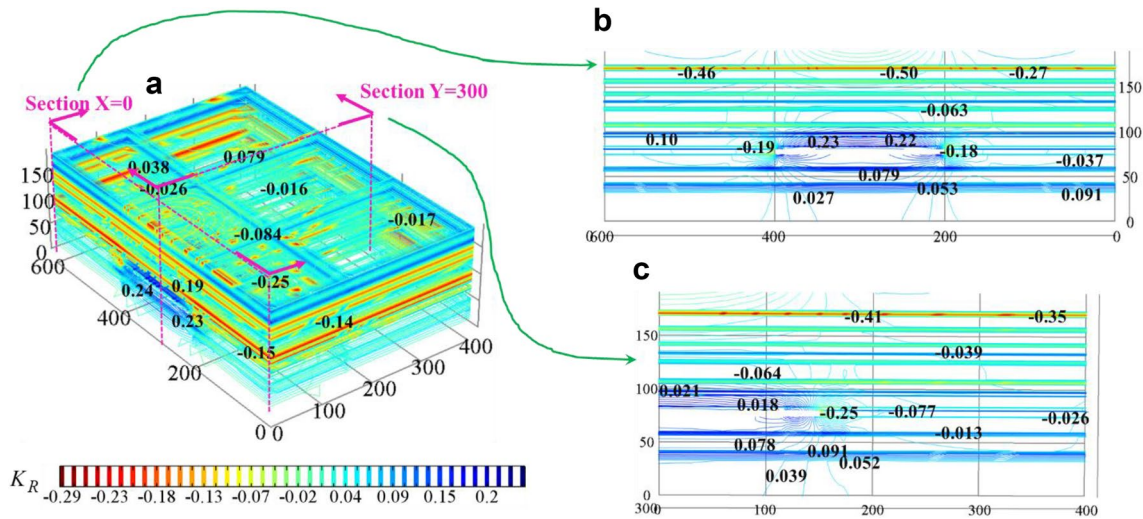
Fig. 12 Modelled distribution contour of the permeability variation rate K_R within the roof and floor strata when the working face advances to 200 m. **a** Three-dimensional distribution of the model, **b** two-dimensional distribution within the section plane $X = 0$, **c** two-dimensional distribution within the section plane $Y = 300$
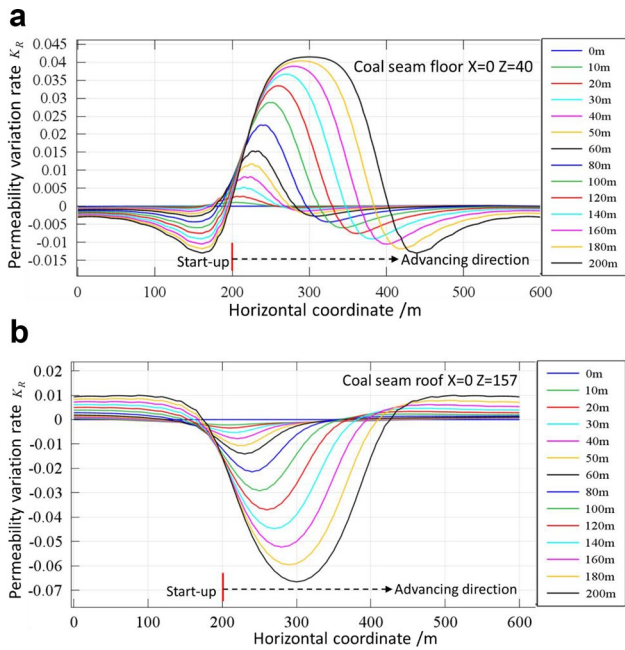

Fig. 13 Modelled permeability variation rate K_R changes with the excavation distance from 0 to 200 m along the monitoring lines. **a** The monitoring line located within the floor strata ($X = 0, Z = 40$), **b** the monitoring line located within the roof strata ($X = 0, Z = 157$)

Fig. 14 Comparison of the flow influx into the excavation region between the measured field data Q_f and the computational data Q_c calculated using the computational models *I*, *II* and *III*

Fig. 15 Comparison of the relative variation of the flow influx Q_δ into the excavation region for the three different computational models

Figure 15 shows that the Q_δ of model *III* ranges from -8 to 23%, which is smaller than models *I* and *II*, which are 20–60% and 81–147%, respectively, indicating that the full Biot poroelastic model that considers changes to the permeability resulting from the excavation-induced stress state variation is better at predicting the actual data than models
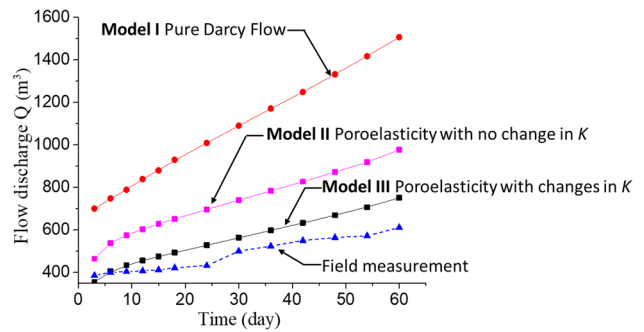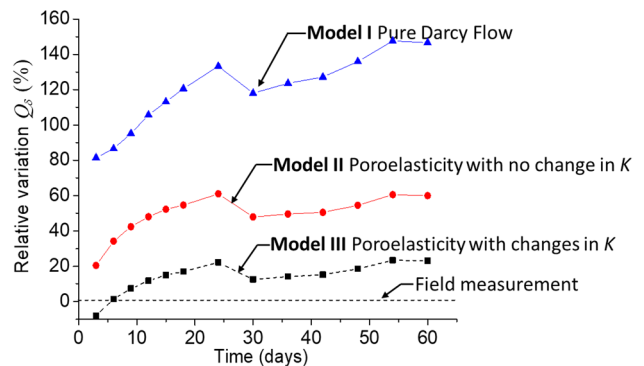
I and *II*. However, the Q_c of the model *III* still has a small disparity from the Q_f, mainly due to factors including the non-uniform mining rate, changes to the geologic conditions and the imprecise selection of model parameters. Through the analysis, we see that the stress sensitivity coefficient β in Eq. (8) is a critical coefficient that largely determines the permeability changes due to the mining-induced stress variations. Thus, an analysis of Q_δ to the stress sensitivity coefficient β was conducted, as shown in Fig. 16. Here, different magnitudes of β, including $0.01\beta, 0.1\beta, 0.5\beta, \beta, 1.5\beta$ and 3β, were chosen for the analysis.

Figure 16 shows that the variation tendency of Q_δ with duration of mining is the same for different stress sensitivity coefficients β. At the same duration of mining, the value of Q_δ decreases with an increase in the magnitude of the coefficient β. After comparison, the Q_δ calculated using 3β is closest to the field measurement, indicating that 3β is the optimal stress sensitivity coefficient and is more suitable for predicting fluid influx into the mining area than β. This is a useful result to help achieve an accurate prediction of fluid influx into an advancing coal mine excavation in the future.

5 Concluding Remarks

The impact of longwall coal mining activities on the underground fluid flow regime is the main concern of geological environmental protection. Three different computational approaches including basic Darcy modelling, complete Biot poroelastic modelling with and without considering permeability changes due to mining-induced stress variations, were used to estimate the fluid inflow into the excavated region as the excavation progresses. Then, a specific case involving the No. 18112 working face of the Xiegou coal mine, located in
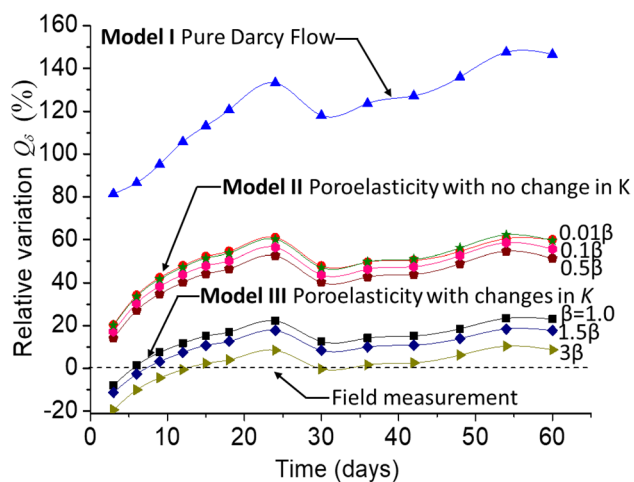

Fig. 16 The sensitivity analysis of the relative variation of flow discharge Q_δ to the stress sensitivity coefficient β

the northwest of the Shanxi province, China, was examined. On the basis of the comprehensive analysis of the geological, hydrologic and mining conditions, a three-dimensional finite element numerical model of the simplified geological model is established using software COMSOL. The mining-induced strata stress changes, permeability variations and fluid influx evolutions with the excavation advancing are analyzed. The differences in modelling results of various methods were analyzed, and different simulation results are compared to the field measurement results. Besides, the sensitivity analysis of the flow influx variations to the stress sensitivity coefficient β, a critical parameter in describing the exponential relation between permeability and strata stress and pore pressure, was conducted.

The Darcy modelling results show that the maximum flow rate usually occurs in the vicinity of the corner regions of the excavation zone at a value of $21.9 \times 10^{-3} \text{m}^3/\text{h}$ and remains unchanged as the mining excavation progresses. Although the stress changes due to mining activities will affect the flow direction of the underground water, the corner regions of the excavation areas always exhibit a greater flow rate. The poroelasticity model with no change in permeability reveals that the zone of relief of the vertical stress is mainly formed in the overlying and underlying strata located above and below the middle of the stope; regions that are far from the excavation space mainly have a larger variation in the vertical stress. Finally, the poroelasticity model that includes changes in permeability indicates that the most significant permeability increases develop in the de-stressed zone, and its significance gradually diminishes and is restricted to a certain distance away from the excavation space, where the permeability even begins to decrease. As the excavation progresses, the increase in the distance mined will result in the larger areas of significant permeability alterations within the overlying and underlying strata close to the excavation; however, there is an opposite influence within the overlying strata that are remote from the excavation.

The comparison between simulation and measured values demonstrated that the Darcy model shows the largest difference from the field measurement data, while the full Biot poroelastic modelling that considers permeability changes gives a good prediction of the fluid flow into the excavation region. A sensitivity analysis of the relative variation in the flow influx to the stress sensitivity coefficient β indicates that the parameter β largely determines fluid influx; the value 3β is the most suitable for predictions of fluid influx into a mining area.

Although the computational modelling of this study was conducted based on a specific geological and mining condition, the research methodology and results are helpful in the comprehensive understanding of the groundwater flow alterations due to the excavation process, especially for coal mines that possess similar geological and mining conditions.

References

Aston TRC, Singh RN (1983) A reappraisal of investigations into strata permeability changes associated with longwall mining. Int J Mine Water 2:1–14

Atkinson C, Craster RV (1991) Plane strain fracture in poroelastic media. Proc R Soc Lond A 434:605–633

Bai M, Elsworth D (1991) An integrated model of fracture flow and solid deformation. In: The 32nd US Symposium on Rock Mechanics (USRMS). American Rock Mechanics Association, Norman, pp 577–586

Biot MA (1941) General theory of three-dimensional consolidation. J Appl Phys 12(2):155–164

Booth CJ (1986) Strata-movement concepts and the hydrogeological impact of underground coal mining. Groundwater 24:507–515

Booth CJ, Spande ED, Pattee CT, Miller JD, Bertsch LP (1998) Positive and negative impacts of longwall mine subsidence on a sandstone aquifer. Environ Geol 34(2–3):223–233

Booth CJ (2006) Groundwater as an environmental constraint of longwall coal mining. Environ Geol 49:796–803

Cheng A-D (2015) Poroelasticity. Springer, Berlin

Christian JT, Desai CS (1977) Constitutive laws for geologic media. In: Christian CSD and JT (ed) Numerical methods in geotechnical engineering. McGraw Hill, New York, p 115

Darve F (2014) Incrementally non-linear constitutive relationships. In: Darve F (ed) Geomaterials constitutive equations and modelling. CRC, London, pp 229–254

David C, Wong T-F, Zhu W, Zhang J (1994) Laboratory measurement of compaction-induced permeability change in porous rocks: implications for the generation and maintenance of pore pressure excess in the crust. Pure Appl Geophys 143(1–3):425–456

Davis RO, Selvadurai APS (2005) Plasticity and geomechanics. Cambridge University Press, Cambridge

Desai CS, Siriwardane HJ (1984) Constitutive laws for engineering materials with emphasis on geologic materials. Prentice-Hall, London

Doulati Ardejani F, Singh RN, Baafi E, Porter I (2003) A finite element model to: 1. Predict groundwater inflow to surface mining excavations. Mine Water Environ 22:31–38

Głowacki A, Selvadurai APS (2016) Stress-induced permeability changes in Indiana limestone. Eng Geol 215:122–130

Guo H, Adhikary DP, Craig MS (2009) Simulation of mine water inflow and gas emission during longwall mining. Rock Mech Rock Eng 42:25–51

Guo H, Yuan L, Shen B et al (2012) Mining-induced strata stress changes, fractures and gas flow dynamics in multi-seam longwall mining. Int J Rock Mech Min Sci 54:129–139

Karaman A, Carpenter PJ, Booth CJ (2001) Type-curve analysis of water-level changes induced by a longwall mine. Environ Geol 40 (7):897–901

Kim J-M, Parizek RR, Elsworth D (1997) Evaluation of fully-coupled strata deformation and groundwater flow in response to longwall mining. Int J Rock Mech Min Sci 34(8):1187–1199

Kiyama T, Kita H, Ishijima Y et al (1996) Permeability in anisotropic granite under hydrostatic compression and triaxial compression including post-failure region. In: 2nd North American rock mechanics symposium. American Rock Mechanics Association, Montreal, pp 1643–1650

Li T, Mei T, Sun X et al (2013) A study on a water-inrush incident at Laohutai coalmine. Int J Rock Mech Min Sci 59:151–159

Liu Z, Hu Y (2007) Solid-liquid coupling study on water inrush through faults in coal mining above confined aquifer. J China Coal Soc 32:1046–1050 **(in Chinese)**

Lu Y, Wang L (2015) Numerical simulation of mining-induced fracture evolution and water flow in coal seam floor above a confined aquifer. Comput Geotech 67:157–171

Mahyari AT, Selvadurai APS (1998) Enhanced consolidation in brittle geomaterials susceptible to damage. Mech Cohesive Frict Mater 3(3):291–303

Nguyen TS, Selvadurai APS (1995) Coupled thermal-mechanical-hydrological behaviour of sparsely fractured rock: implications for nuclear fuel waste disposal. Int J Rock Mech Min Sci Geomech Abstr 32(5):465–479

Ouyang Z, Elsworth D (1993) Evaluation of groundwater flow into mined panels. Int J Rock Mech Min Sci 30:71–79

Özgen Karacan C, Goodman G (2009) Hydraulic conductivity changes and influencing factors in longwall overburden determined by slug tests in gob gas ventholes. Int J Rock Mech Min Sci 46:1162–1174

Pietruszczak S (2010) Fundamentals of plasticity in geomechanics. CRC, Boca Raton

Qiao X, Li G, Li M et al (2011) Influence of coal mining on regional karst groundwater system: a case study in West Mountain area of Taiyuan City, northern China. Environ Earth Sci 64:1525–1535

Rapantova N, Grmela A, Vojtek D et al (2007) Ground water flow modelling applications in mining hydrogeology. Mine Water Environ 26:264–270

Rice JR, Cleary MP (1976) Some basic stress diffusion solutions for fluid-saturated elastic porous media with compressible constituents. Rev Geophys 14(2):227–241

Selvadurai APS (ed) (1996) Mechanics of poroelastic media. Kluwer Academic, The Netherlands

Selvadurai APS (2004) Stationary damage modelling of poroelastic contact. Int J Solids Struct 41(8):2043–2064

Selvadurai APS (2007) The analytical method in geomechanics. Appl Mech Rev 60(3):87–106

Selvadurai APS (2018) The Biot coefficient for a low permeability heterogeneous limestone. Contin Mech Thermodyn 1–15

Selvadurai APS, Boulon MJ (1995) Mechanics of geomaterial interfaces. Studies in applied mechanics, vol 42. Elsevier, Amsterdam

Selvadurai APS, Głowacki A (2008) Permeability hysterisis of limestone during isotropic compression. Groundwater 46(1):113–119

Selvadurai APS, Głowacki A (2017) Stress-induced permeability alterations in an argillaceous limestone. Rock Mech Rock Eng 50(5):1079–1096

Selvadurai APS, Kim J (2016) Poromechanical behaviour of a surficial geological barrier during fluid injection into an underlying poroelastic storage formation. Proc R Soc A 472:20150418

Selvadurai APS, Najari M (2016) Isothermal permeability of the argillaceous Cobourg Limestone. Oil Gas Sci Technol d'IFP Energ Nouv 71(4):53

Selvadurai APS, Najari M (2017) The thermo-hydro-mechanical behavior of the argillaceous Cobourg Limestone. J Geophys Res Solid Earth 122(6):4157–4171

Selvadurai APS, Nguyen TS (1995) Computational modelling of isothermal consolidation of fractured porous media. Comput Geotech 17:39–73

Selvadurai APS, Selvadurai PA (2010) Surface permeability tests: experiments and modelling for estimating effective permeability. Proc R Soc A 466:2819–2846

Selvadurai PA, Selvadurai APS (2014) On the effective permeability of a heterogeneous porous medium: the role of the geometric mean. Philos Mag 94(20):2318–2338

Selvadurai APS, Shirazi A (2004) Mandel–Cryer effects in fluid inclusions in damage-susceptible poroelastic geologic media. Comput Geotech 31:285–300

Selvadurai APS, Shirazi A (2005) An elliptical disc anchor in a damage-susceptible poroelastic medium. Int J Numer Methods Eng 63:2017–2039

Selvadurai APS, Suvorov AP (2012) Boundary heating of poro-elastic and poro-elasto-plastic spheres. Proc R Soc A 468:2779–2806

Selvadurai APS, Suvorov AP (2014) Thermo-poromechanics of a fluid-filled cavity in a fluid-saturated geomaterial. Proc R Soc A 470(2163):20130634

Selvadurai APS, Suvorov AP (2016) Thermo-poroelasticity and geomechanics. Cambridge University Press, Cambridge

Selvadurai APS, Suvorov AP, Selvadurai PA (2015) Thermo-hydro-mechanical processes in fractured rock formations during a glacial advance. Geosci Model Dev 8:2167–2185

Shi W, Yang T, Yu Q et al (2017) A study of water-inrush mechanisms based on geo-mechanical analysis and an in-situ groundwater investigation in the Zhongguan iron mine, China. Mine Water Environ 36:409–417

Shiping L, Yushou L, Yi L et al (1994) Permeability-strain equations corresponding to the complete stress—strain path of Yinzhuang sandstone. Int J rock Mech Min Sci Geomech Abstr 31(4):383–391

Skempton AW (1954) The pore pressure coefficients A and B. Geotechnique 4(4):143–147

Sun W, Wu Q, Dong D, Jiao J (2012) Avoiding coal–water conflicts during the development of China's large coal-producing regions. Mine Water Environ 31(1):74–78

Surinaidu L, Gurunadha Rao VVS, Srinivasa Rao N, Srinu S (2014) Hydrogeological and groundwater modeling studies to estimate the groundwater inflows into the coal Mines at different mine development stages using MODFLOW, Andhra Pradesh, India. Water Resour Ind 7:49–65

Tan D (2013) Water for coal: thirsty miners. China water risk website. Retrieved from http://chinawaterrisk.org/resources/analysis-reviews/water-for-coal-thirsty-miners-feel-the-pain/. Retrieved 9 Apr 2018.

Wang JA, Park HD (2003) Coal mining above a confined aquifer. Int J Rock Mech Min Sci 40(4):537–551

Yue ZQ, Selvadurai APS (1995) Contact problem for saturated poroelastic solid. J Eng Mech 121(4):502–512

Zeng Y, Wu Q, Liu S et al (2017) Evaluation of a coal seam roof water inrush: case study in the Wangjialing coal mine, China. Mine Water Environ 37(1):1–11

Zhang D, Fan G, Liu Y, Ma L (2010) Field trials of aquifer protection in longwall mining of shallow coal seams in China. Int J Rock Mech Min Sci 47(6):908–914

Zhang R, Ning Z, Yang F et al (2016) A laboratory study of the porosity–permeability relationships of shale and sandstone under effective stress. Int J Rock Mech Min Sci (81):19–27

Zhao Y (2010) Multi-field coupling and engineering response of porous media. Science, Beijing **(in Chinese)**

Zhu WC, Wei CH (2011) Numerical simulation on mining-induced water inrushes related to geologic structures using a damage-based hydromechanical model. Environ Earth Sci 62(1):43–45

Zhu B, Wu Q, Yang J, Cui T (2014) Study of pore pressure change during mining and its application on water inrush prevention: a numerical simulation case in Zhaogezhuang coalmine, China. Environ Earth Sci 71(5):2115–2132